Multifractal Analysis of Temporal Variation in Soil Pore Distribution

Yanhui Jia [1], Yayang Feng [2], Xianchao Zhang [3] and Xiulu Sun [2,4,*]

1 Shandong Provincial University Laboratory for Protected Horticulture, Weifang University of Science and Technology, Weifang 262700, China; jyh_5151@126.com
2 Institute of Farmland Irrigation, Chinese Academy of Agricultural Sciences, Xinxiang 453002, China
3 Power China of Beijing Engineering Corporation Limited, Beijing 100024, China
4 Key Laboratory of Water-Saving Agriculture of Henan Province, Xinxiang 453002, China
* Correspondence: sunxiulu@caas.cn

Abstract: Soil structure, a critical indicator of soil quality, significantly influences agricultural productivity by impacting on the soil's capacity to retain and deliver water, nutrients, and salts. Quantitative study of soil structure has always been a challenge because it involves complex spatial-temporal variability. This study employs multifractal analysis to assess the temporal variation in soil pore distribution, a pivotal factor in soil structure. Field observation data were collected in a sandy loam area of the People's Victory Canal Irrigation scheme in Henan Province, China. A 200 m × 200 m test plot with five sampling points was used to collect soil samples at three depth layers (10–30 cm, 30–50 cm, and 50–70 cm) for soil water retention curve and particle size composition analysis, with a total of seven sampling events throughout the growing season. The results revealed that while soil particle-size distribution (Particle-SD) showed minor temporal changes, soil pore-size distribution (Pore-SD) experienced significant temporal fluctuations over a cropping season, both following a generalized power law, indicative of multifractal traits. Multifractal parameters of Pore-SD were significantly correlated with soil bulk density, with the strongest correlation in the topsoil layer (10–30 cm). The dynamic changes in soil pore structure suggest potential variations during saturation–unsaturation cycles, which could be crucial for soil water movement simulations using the Richards equation. The study concludes that incorporating time-varying parameters in simulating soil water transport can enhance the accuracy of predictions.

Keywords: soil structural variability; soil porosity; multifractal characteristics; soil water movement

1. Introduction

Soil provides a nurturing environment for crops, and a suitable edaphic condition can effectively promote crop growth, thereby achieving high yields [1,2]. The structure of soil, as one of the key indicators of soil quality, holds significant importance. The quality of soil structure is directly related to its physical, chemical, and biological properties, which collectively determine the soil's ability to retain and supply water, nutrients, and gases [3]. The stability and suitability of soil structure have a profound impact on crop root development, water and nutrient absorption, and soil microbial activity [4]. Changes in the natural conditions, such as extreme rainfall and freeze–thaw, can affect soil structure [5]. Additionally, various human activities, including tillage, fertilization, irrigation, and changes in land use, can also have direct or indirect impacts on soil structure [6]. These impacts may lead to the

degradation of soil structure, such as compaction, erosion, and a decline in organic matter content, thereby affecting the soil's basic properties, including water retention, supply, and permeability [7].

Moreover, soil structure plays a decisive role in the dynamic changes and distribution of soil water movement. Understanding the impact of soil structure on water movement is of great significance for the management of soil moisture in farmlands and the guidance of crop irrigation [5]. At the same time, the transport of salt and solute in the soil is also closely related to soil structure [8]. The pore characteristics of soil structure determine the diffusion and migration rates of solutes in the soil, which in turn affect soil fertility and the growth environment for crops [9]. Therefore, quantitative research on soil structure is not only conducive to an in-depth understanding of the mechanisms of soil water and solute transport, but also has important practical significance for optimizing farmland management, improving crop yield and quality, and protecting the soil environment [10].

The complexity and variability of soil structure are among its most notable characteristics. Numerous studies have shown that soil structure exhibits significant spatial variability [11], and this variability changes over time [12]. Agricultural activities such as tillage, irrigation, and crop growth all impact soil structure, causing it to display different characteristics at different points in time. This temporal variability makes the study of soil structure more complex and challenging.

In the study of soil structure, direct observation and indirect methods are the two main approaches. Direct observation methods allow for the visual inspection of soil pore structures, including the use of computed tomography (CT) scanning technology, optical microscopy, and electron microscopy to observe thin soil sections and soil fracture surfaces [13]. These methods provide intuitive images of soil pores, helping researchers understand the shape, size, and distribution of soil pores. In particular, CT scanning technology, as a non-destructive testing method, allows for observation without damaging the soil sample. However, despite the potential of CT scanning technology in soil structure research, its measurement accuracy still needs improvement, especially in detecting tiny pores in the soil, which limits its effectiveness in practical applications [14].

On the other hand, indirect methods infer the soil structure through physical or chemical means. Common indirect methods include the penetration curve method and the soil water retention curve method. The penetration curve method indirectly infers the size and distribution of soil pores by measuring the soil's transmission capacity for particles of different sizes [15]. This method is simple and easy to perform but may be affected by the soil's moisture state and the surface properties of the particles. The soil water retention curve method, on the other hand, measures the water release characteristics of the soil at different water contents, indirectly reflecting the water retention capacity of the soil pores [16]. This method can reveal the mechanisms of soil water movement and help understand the retention and release characteristics of soil moisture. Although indirect methods cannot provide direct images of soil pores, they can provide useful soil structure information in certain situations and are an important supplementary means for studying soil pore structures.

Quantitative study of soil structure has always been a challenge because it involves complex spatial scales and multidimensional variability. However, with the introduction of advanced theories such as fractal theory, stochastic theory, and geo-statistics, the field of soil science has made significant progress in the quantitative research of soil structure. Fractal theory is particularly suitable for studying the spatial variability of soil structure at different scales, providing a tool that can quantitatively characterize complexities from micro to macro scales [17].

The essence of fractal methods lies in their ability to describe complex geometric shapes with self-similar properties [18]. In soil science, this approach has been extended to describe the multi-fractal dimensions of soil particles and pore structures, rather than a single fractal dimension [19,20]. This extended method is known as the multi-fractal spectrum, which allows researchers to analyze the complexity of soil structure in greater detail. The variability characterization method based on the multi-fractal spectrum, namely multi-fractal analysis, has been applied to soil research and has shown its great potential [21–23].

Multifractal analysis, by employing multifractal methods to study soil, reveals the complexity of soil particle and pore structures. Research indicates that the distribution of soil particles and pores does not follow a single power-law distribution but exhibits characteristics of a generalized power law, implying that they possess multifractal properties [24]. This discovery is significant for understanding the spatial heterogeneity of soil structure and its impact on soil physical, chemical, and biological processes. Through this analysis, researchers are able to more accurately predict and simulate the transport processes of soil water, nutrients, and gases, thereby providing a scientific basis for soil management and agricultural practices.

Under the influence of tillage, irrigation, rainfall, and evaporation, soil continuously undergoes alternating wet and dry cycles: it shrinks when losing water, leading to the formation of cracks on the soil surface due to volume reduction; and expands when absorbing water, causing soil cracks to close as the volume increases. This process of shrinkage and swelling significantly alters the soil pore structure and distribution, thereby changing the patterns of soil water movement. The wet and dry cycling promotes the formation of soil aggregates and changes the soil pore structure, resulting in distinct spatiotemporal variability in the soil's hydrological and thermal properties. It is, then, crucial to study the temporal variation patterns of soil physical properties for enhancing the accuracy of simulation results and predictive outcomes.

Therefore, the objective of this paper is (1) to analyze the composition of soil particles by applying multifractal analysis and (2) to quantitatively describe the temporal variability of soil pore distribution inferred from soil water retention curves. This study can provide theoretical support for the simulation of soil water movement.

2. Materials and Methods

2.1. The Study Area and Experimental Design

The field observation data were collected in the People's Victory Canal Irrigation scheme, which is located in Henan Province, China (35°08′ N, 113°45′ E). The study area has a temperate continental monsoon climate, with an average annual temperature of 14 °C, an average annual rainfall of 656.3 mm, and an average annual evaporation of 1748.4 mm. The precipitation pattern is concentrated mostly from June to September, accounting for 72% of the total annual rainfall. The study area encompasses approximately 4 hm^2 of land, with a predominant soil type of sandy loam. The soil bulk density is 1.52 g/cm^3 with an average porosity of 45.57%. The field capacity is 31.52% (volumetric water content), and the organic matter content is about 1.2% on average. The crop pattern throughout the study area is dominated by summer maize (mid-June to late September) and winter wheat (early October to mid-June of the following year).

A test plot of 200 m wide and 200 m long was selected in the field, with 5 sampling points established. Soil samples were taken in a 1.5 m × 1.5 m grid. After removing the top 10 cm of soil, sampling was conducted at 10–30 cm as Layer 1, 30–50 cm as Layer 2, and 50–70 cm as Layer 3. Soil samples for determining the soil water retention curve were taken using a 60 cm^3 ring knife (inner diameter 61.8 mm, height 2 cm), and soil particle size composition samples were collected in sealed bags. Five sampling points were set up in

the direction from north to south (as shown in Figure 1), with five samples taken from each layer at each sampling point, resulting in a total of 15 soil samples per layer and 75 soil samples from all five sampling points per sampling event. Sampling times were before tillage on 10 October 2021, after sowing on 23 November 2021, after the first irrigation on 24 December 2021, after the second irrigation on 11 February 2022, after the third irrigation on 4 March 2022, after the fourth irrigation on 8 April 2022, and before harvest on 13 May 2022, with a total of seven soil sampling events.
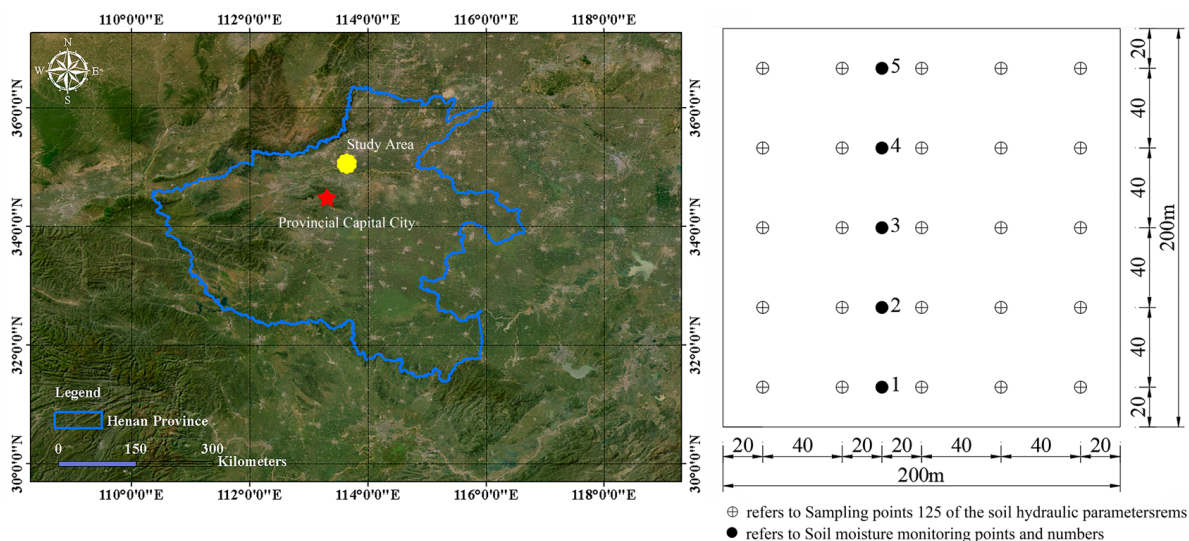

Figure 1. The location of the study area and the experimental layout.

(1) Determination of Soil Bulk Density. Soil bulk density during the wheat season was measured using the ring knife method, where soil samples were dried in an oven at 105 °C until constant mass was achieved (drying for over 12 h). The dry soil mass was then divided by the volume of the ring knife to obtain the initial soil bulk density.

(2) Determination of Soil Particle Size. Large particles in the original soil samples were dispersed and crushed, air-dried, and passed through a 0.9 mm sieve. The soil samples were then measured in a BT-9300H(T)type laser particle size analyzer (Bettersize Instruments LTD., Dandong, Liaoning, China) with a measurement range of 0.1 to 1000 µm. To reduce experimental error, each soil sample was measured five times, and the average value was taken. According to the U.S. standard classification, clay particles are less than 2 µm in size, silt particles range from 2 to 50 µm, and sand particles range from 50 to 1000 µm.

(3) Soil water retention curve. The pressure plate extractor (Soilmoisture Equipment Corp., Santa Barbara, CA, USA) was used for the measurement. The pressure system of the membrane apparatus applied different pressures to the soil samples, ranging from 0 to 15 bar. When the drainage stopped for more than 24 h, it indicated that the soil moisture was completely drained at that pressure value, and the sample was weighed before proceeding to the next pressure value. After all pressure values were measured, the soil samples were dried in an oven, and the dry bulk density of each sample was determined.

2.2. Young–Laplace Equation

The matric suction of unsaturated soil is defined as [25]:

$$\phi = u_a - u_w \tag{1}$$

where u_a is the pore air pressure, and u_w is the pore water pressure.

The Young–Laplace equation for unsaturated soil can be written as [16]

$$\phi = \frac{2\sigma_{aw}\cos\theta}{r} \tag{2}$$

where σ_{aw} is the air–water interfacial tension, ϕ is the contact angle between the water and the capillary surface, and r is the radius of the capillary.

When the matric suction is expressed by water head, Formula (2) can be written as

$$\phi_h = \frac{2\sigma_{aw}\cos\theta}{\rho_w g r} \tag{3}$$

where ρ_w is density of water, and g is gravitational acceleration.

2.3. Multifractal Analysis

To implement the scaling analysis of a general mass distribution and measure µ supported on the interval I = [a, b], a set of different meshes with cells or subintervals of I with equal length is required. A common choice is to consider dyadic scaling down, that is, successive partitions of the interval I of size $\varepsilon = 2^{-k}L$, where L is the length of I, and $k = 0$, 1, 2... At each size scale ε, a number $N(\varepsilon) = 2^k$ of cells is considered and their respective measures $\mu(\varepsilon)$ are found from the data.

The number $\log\mu_i/\log\varepsilon$ is the singularity strength of the ith cell. This exponent can be interpreted as a crowding index or a degree of concentration of μ: the greater this value is, the smaller is the concentration of the measure, and vice versa.

Multifractal analysis aims to find scaling parameters or dimensions for characterizing measures displaying high irregularity or variation of singularity strength values. The Shannon entropy (H) of the measure is defined by

$$H(\varepsilon) = -\sum_{i=1}^{N(\varepsilon)} \mu_i(\varepsilon)\log\mu_i(\varepsilon) \tag{4}$$

H is a measure of heterogeneity or unevenness of the measure. When the limit

$$D_E = \lim_{\varepsilon \to 0} \frac{\sum_{i=1}^{N(\varepsilon)} \mu_i(\varepsilon)\log\mu_i(\varepsilon)}{\log\varepsilon} \tag{5}$$

exists, its value is called the entropy dimension or information dimension of the distribution [26], quantifying the growth rate of the entropy with respect to ε. This expression can be seen as the l-weighted average of the singularity strength values. It is also related to the size level (dimension) of the minimal set where the whole measure is concentrated [27].

The entropy dimension DE is a special case of the Rényi dimensions defined by

$$D_q = \frac{1}{q-1}\lim_{\varepsilon \to 0}\frac{\log\sum_{i=1}^{N(\varepsilon)}\mu_i(\varepsilon)^q}{\log\varepsilon} \tag{6}$$

3. Results

3.1. Soil Particle-Size Distribution (Particle-SD)

It can be observed from Figure 2 that the soil particle contents in various size intervals obtained multiple times were generally consistent, with the coefficient of variation (CV) of the soil particle content in most intervals being less than 20%. Only in intervals with low soil particle contents, the CV is relatively high. Notably, Layer 1 exhibits lower variability compared to Layer 2 and Layer 3. These observations suggest that the soil

particle composition in the plot has undergone minor changes, indicating a relatively uniform soil texture.
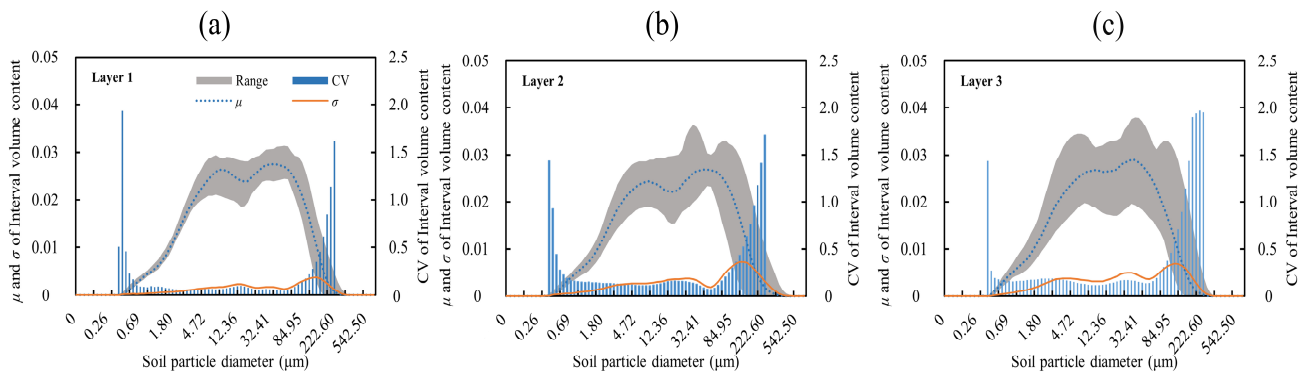

Figure 2. The mean value, variance, and CV of soil particle content in various diameter intervals ((**a**) refers to the soil layer 1 at 10–30 cm, (**b**) refers to the soil layer 2 at 30–50 cm and (**c**) refers to the soil layer 3 at 50–70 cm).

The statistical results of soil particle size composition at various sampling points indicate that processes such as tillage, sowing, and irrigation have a minimal overall impact on the soil particle size of the test samples. The CV for clay and silt particles generally shows weak variability, with some data exhibiting larger variations in the CV, which are attributed to measurement errors. The CV for sand particles generally indicates moderate variability, suggesting that soil water movement has caused some transport and loss of sand particles.

3.2. Multifractal Analysis of Soil Particle-SD

The q-D(q) generalized dimension spectra exhibit a curvilinear shape (Figure 3). Within the range of $-10 \leq q \leq 10$, the curve monotonically decreases as the value of q increases, i.e., D(0) > D(1) > D(2), indicating that the soil particle composition conforms to multifractal characteristics. A greater degree of curvature in the curve corresponds to a stronger heterogeneity in the distribution of soil particles. When q is positive, the dimensional analysis quantifies the behavior of dense regions; conversely, when q is negative, it quantifies the behavior of sparse regions. The curve of D(q) changes rapidly and exhibits a greater degree of curvature when q is negative, whereas the curve is relatively flat when q is positive. This observation suggests that the distribution of soil particles in sparse regions is more sensitive than that in dense regions.
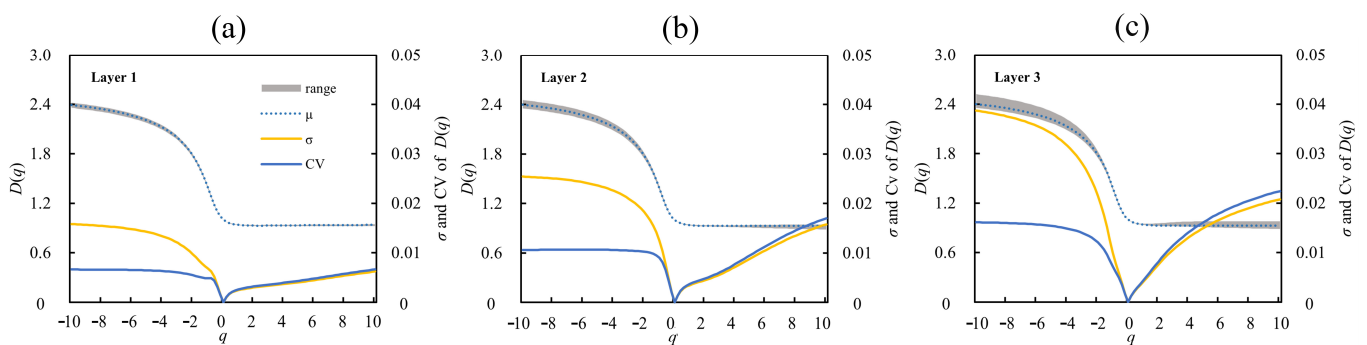

Figure 3. The mean value, variance, and CV of the generalized fractal dimension spectrum D(q) of the particle composition of various soil samples ((**a**) refers to the soil layer 1 at 10–30 cm, (**b**) refers to the soil layer 2 at 30–50 cm and (**c**) refers to the soil layer 3 at 50–70 cm).

Based on the range of D(q) distribution, σ, and CV values shown in the graph, it can be observed that the multifractal D(q) values of each soil sample vary slightly, with CV values less than 2.5%, indicating low variability. In addition, Layer 1 has lower D(q) values compared to Layer 2 and Layer 3, which is consistent with the soil particle-size distribution results mentioned in Section 3.1.

The multifractal spectrum α-f(α) can provide more information on the characteristics of soil particle composition. The multifractal spectra of soil particle composition in different layers are shown in Figure 4. It can be observed that the multifractal singularity spectra α-f(α) of the soil particle composition distribution are continuous and convex, and all curves show asymmetry, indicating that the soil particle composition distribution at each layer of all sampling points is uneven, with some particle sizes having higher contents while others having lower contents. The shape of the α-f(α) curve is left-skewed, indicating that the soil particle distribution is more concentrated. The error bars, σ, and CV of the α-f(α) curves indicate that the particle composition of each soil sample is relatively consistent.
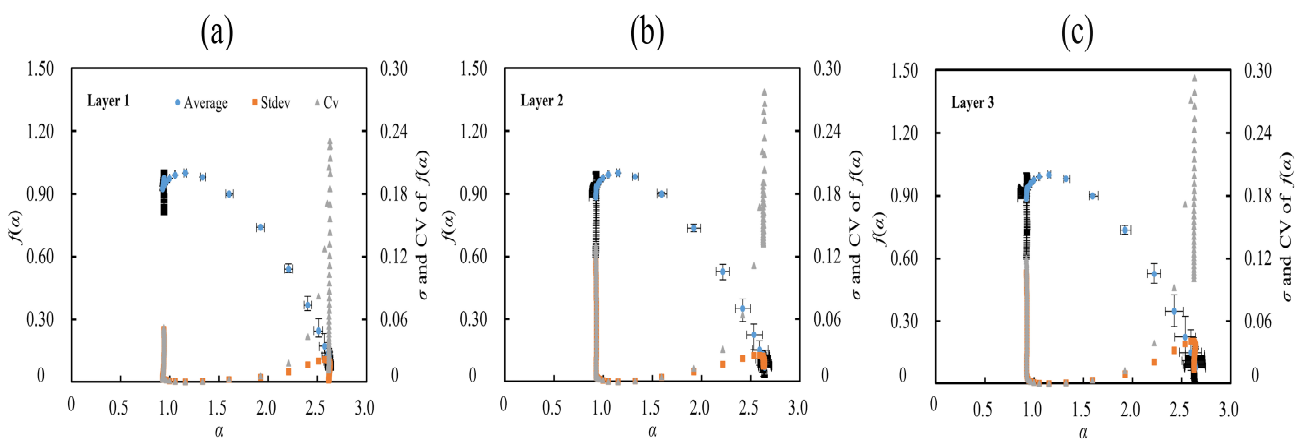

Figure 4. The mean value, variance, and CV of the multifractal spectrum of the particle composition of various soil samples (error bar represents the standard deviation; (**a**) refers to the soil layer 1 at 10–30 cm, (**b**) refers to the soil layer 2 at 30–50 cm and (**c**) refers to the soil layer 3 at 50–70 cm).

As is shown in Figure 5, D1 is the information entropy dimension, which is related to the entropy value of the system and can be used to characterize the heterogeneity of soil particle distribution. A higher D1 value indicates a wider distribution range and stronger heterogeneity of soil particles. The D1 values of each soil sample are around 0.9, with little difference.
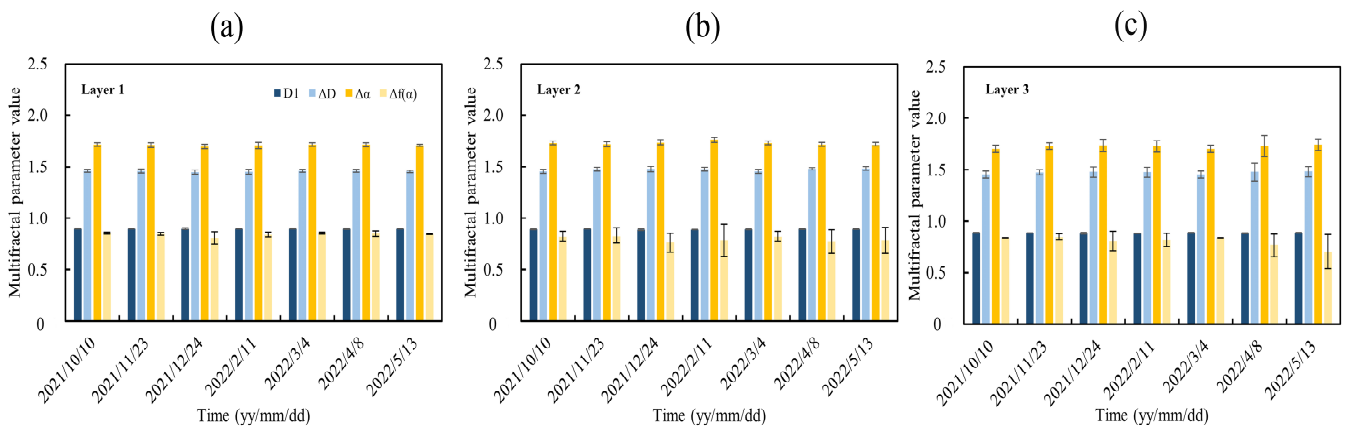

Figure 5. The bar chart of D1, ΔD, Δα, and Δf for the particle composition of various soil samples (error bar represents the standard deviation; (**a**) refers to the soil layer 1 at 10–30 cm, (**b**) refers to the soil layer 2 at 30–50 cm and (**c**) refers to the soil layer 3 at 50–70 cm).

ΔD = D(−10) − D(10), which represents the curvature degree of the generalized dimension spectrum curve, and ΔD value reflects the degree of variation of local features of soil particle distribution. The larger the ΔD value, the stronger the variation degree of soil particles. The ΔD values of each soil sample are around 1.45, with little variance.

Δα = αmax − αmin, which represents the width of the multifractal spectrum. Δα characterizes the features of different hierarchical structures of the research object and reflects the degree of non-uniformity of the probability measure of multifractal physical quantities in the research range. A larger Δα value indicates a more complex diameter distribution of soil particles and a higher non-uniformity.

Δf = f(αmin) − f(αmax), which reflects the shape characteristics of the multifractal spectrum. When Δf > 0, the major subsets are dominant, and the multifractal singularity spectrum function exhibits a left hook shape. When Δf < 0, the minor subsets are dominant, and the multifractal singularity spectrum function exhibits a right hook shape.

In general, both the values of Δα and Δf for the soil particle diameter distribution among the three soil layers and the seven sampling times show little variation, indicating that the soil particle composition does not change significantly over time, and the distribution non-uniformity is comparable among the different layers.

3.3. Soil Porosity Distribution

Figure 6 shows the evolving distribution of soil porosity (averaged over five points) in each soil layer over time. Figure 6a represents Layer 1, showing a sharp peak in pore volume content around 20 μm, indicating a high prevalence of pores in this size range, with minimal variability across different dates. Figure 6b depicts Layer 2, where the peak is less pronounced and occurs at a slightly larger pore radius, suggesting some variability in pore-size distribution over time. Figure 6c corresponds to Layer 3, exhibiting a broader peak at an even larger pore radius, with significant variability in pore-size distribution across the dates.
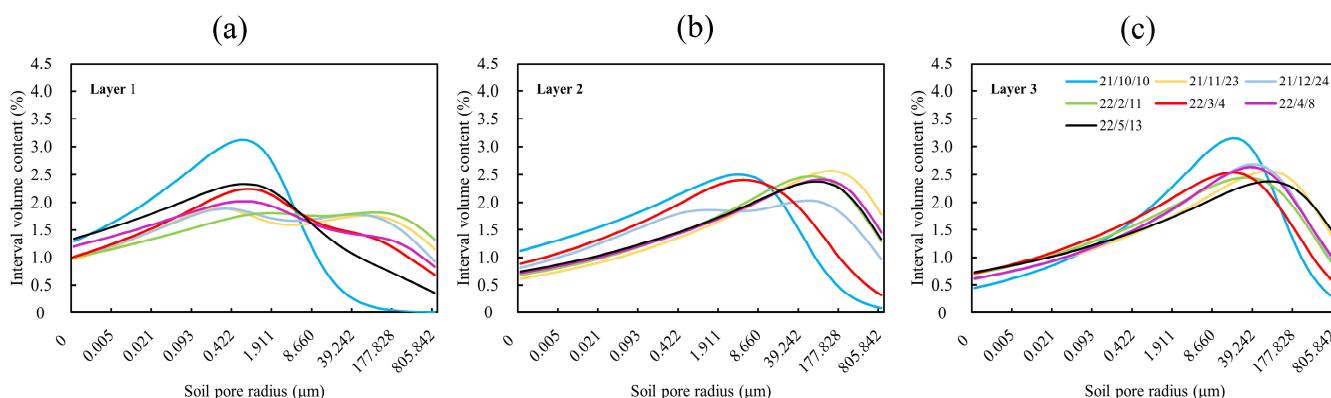

Figure 6. Soil pore distribution (average) at various sampling times ((**a**) refers to the soil layer 1 at 10–30 cm, (**b**) refers to the soil layer 2 at 30–50 cm and (**c**) refers to the soil layer 3 at 50–70 cm).

The variation trends across the three layers exhibit a degree of consistency. Specifically, the contents of both small- and medium-sized pores demonstrate a shift from high values prior to tillage (10 October 2021) to lower values post-tillage (23 November 2021), and progressively increased with greater irrigation frequency and crop growth. Conversely, the contents of large pores increased after tillage, followed by a gradual decrease. Notably, the extent of these changes diminishes as the sampling depth increases.

The data points for pore radius are consistent across all layers, providing a standardized basis for comparison. The analysis reveals that soil pore-size distribution is relatively stable in the top layer but shows more temporal variability in the middle and bottom layers,

which could be influenced by water movement, compaction, or biological activity. This information is essential for understanding soil physical properties that affect water retention, aeration, and root growth, thereby impacting soil health and agricultural productivity.

3.4. Multifractal Analysis of Soil Porosity

The q-D(q) generalized dimension spectrum exhibits a curvilinear shape (Figure 7). Within the range of $-10 \leq q \leq 10$, the curve monotonically decreases as the value of q increases, i.e., D(0) > D(1) > D(2), indicating that the soil porosity composition conforms to multifractal characteristics. The curve of D(q) changes rapidly and exhibits a greater degree of curvature when q is negative, whereas the curve is relatively flat when q is positive. This observation suggests that the distribution of soil particles in sparse regions is more sensitive than that in dense regions.
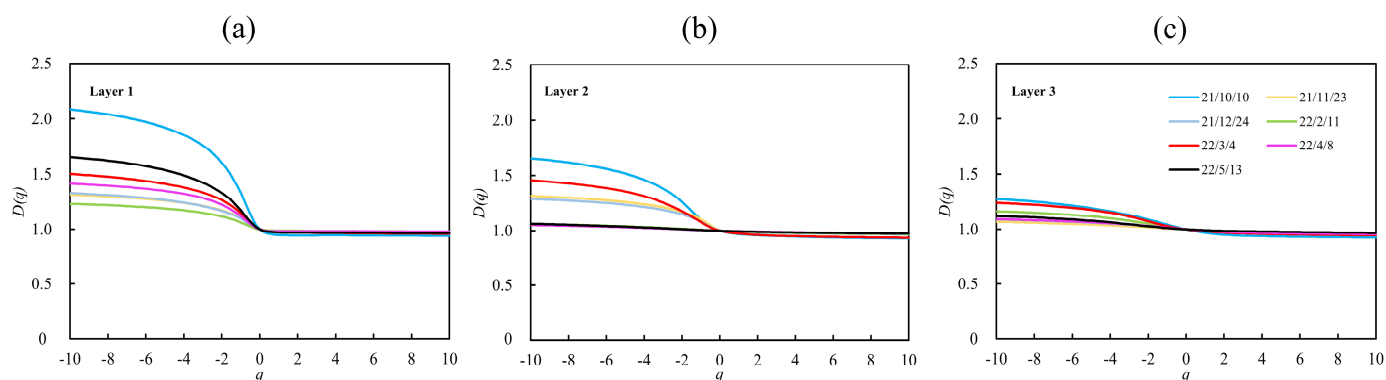

Figure 7. The generalized fractal dimension spectrum D(q) curves for the soil pore distribution of various soil samples ((**a**) refers to the soil layer 1 at 10–30 cm, (**b**) refers to the soil layer 2 at 30–50 cm and (**c**) refers to the soil layer 3 at 50–70 cm).

By assessing the curvature of D(q) distribution curves, a consistent trend is observed in the generalized dimension spectra of soil porosity across three distinct layers. These spectra exhibit a transition from a substantial degree of curvature before the tillage event (on 10 October 2021) to a less pronounced curvature after tillage (on 23 November 2021). Subsequently, they gradually reverted to a more pronounced curvature with increased irrigation frequency and crop growth. Notably, as the sampling depth increases, the magnitude of these variations gradually diminishes.

The multifractal spectrum α-f(α) provides a deeper understanding of the compositional features of soil porosity. The multifractal spectrum functions α-f(α) for different soil layers at various sampling times are depicted in Figure 8. From this graph, it is evident that the multifractal spectra of soil porosity composition exhibit continuous convex curves, with each set of curves displaying asymmetry. This observation suggests that the soil porosity composition at all sampling points and layers is non-uniform, with certain pore size contents being higher while others are lower. The α-f(α) graphs show a left-skewed shape, indicating a relatively concentrated distribution of soil porosity.

Further analysis of the α-f(α) graphs for soil porosity in the three layers demonstrates a consistent temporal trend. The spectra transition from prominent spans and curvatures before tillage (on 10 October 2021) to more modest spans and curvatures after tillage (on 23 November 2021). As irrigation frequency increases and crop growth progresses, the spectra gradually shift towards larger spans and more pronounced curvatures. It is worth noting that the magnitude of these changes gradually decreases with the deepening of the sampling depth.
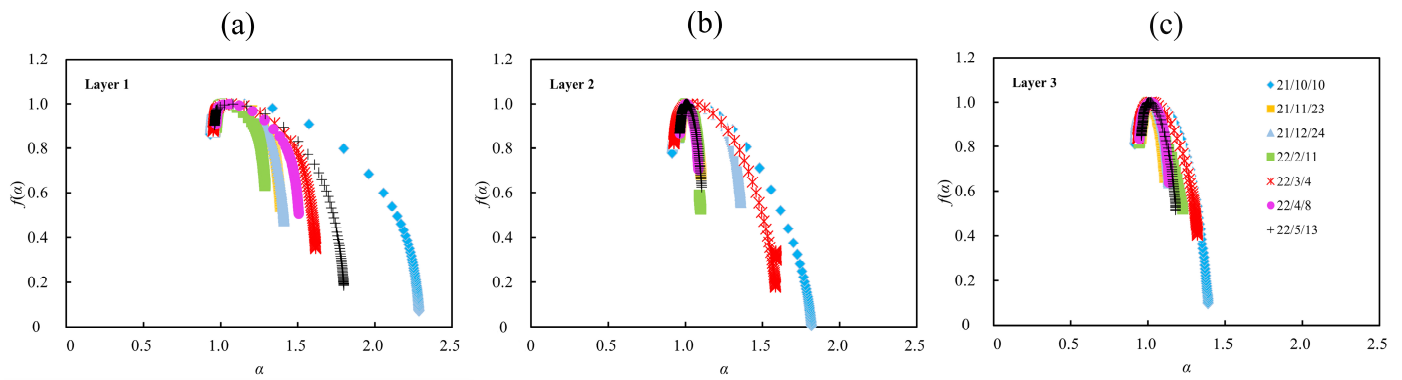
Figure 8. The multifractal spectra f(α) curves of soil pores for various soil samples ((**a**) refers to the soil layer 1 at 10–30 cm, (**b**) refers to the soil layer 2 at 30–50 cm and (**c**) refers to the soil layer 3 at 50–70 cm).

In Figure 9, D(1) represents the information entropy dimension, and the D(1) values for all soil samples fall within the range of 0.9 to 1.0, exhibiting minimal variation. However, with varying sampling times, D(1) generally demonstrates an increasing trend followed by a decrease. This suggests that tillage practices expanded the soil distribution range. As the soil depth increases, this trend becomes less pronounced, indicating that the impact of tillage on the heterogeneity of pore distribution diminishes with increasing soil depth.
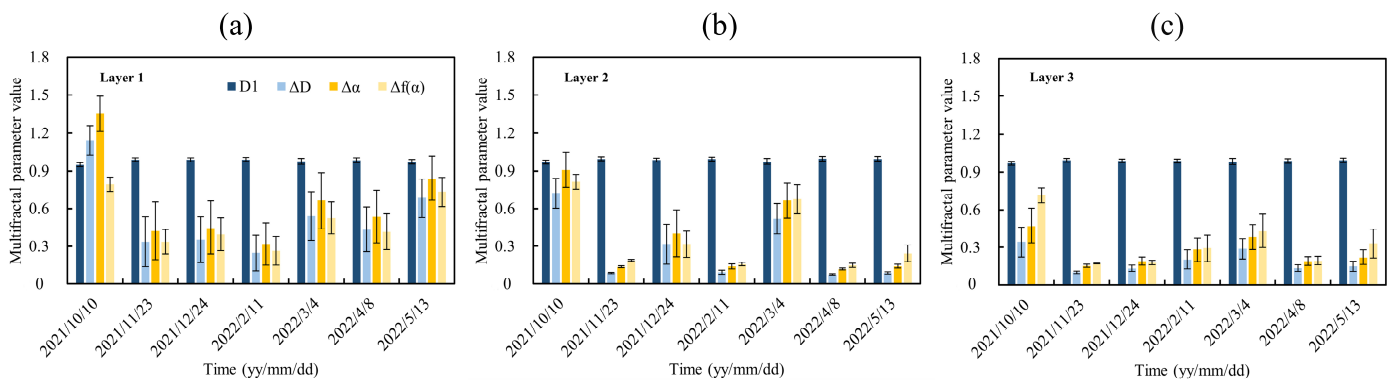

Figure 9. The bar chart of D1, ΔD, $\Delta\alpha$, and Δf for the soil pore distribution of various soil samples (error bar represents the standard deviation; (**a**) refers to the soil layer 1 at 10–30 cm, (**b**) refers to the soil layer 2 at 30–50 cm and (**c**) refers to the soil layer 3 at 50–70 cm).

ΔD = D(−10) − D(10), which represents the curvature of the generalized dimension curve. From the graph, ΔD primarily exhibits a decreasing trend followed by an increase. This indicates that tillage reduced the complexity and non-uniformity of pore distribution. With increasing soil depth, this trend becomes less apparent, signifying that the impact of tillage on the variability of local pore distribution characteristics decreases with soil depth.

$\Delta\alpha$ = αmax − αmin, representing the width of the multifractal spectrum. Overall, the $\Delta\alpha$ values for soil particle distribution from seven sampling events across three soil layers generally show a trend of decreasing followed by an increase. This suggests that, over time, the complexity of soil particle composition shifts from high complexity before tillage to low complexity after tillage, and then gradually returns to a state of high complexity with following irrigation and root growth. As the soil depth increases, this trend becomes less pronounced.

Δf = f(αmin) − f(αmax). It is evident from Figure 9 that when Δf > 0, the soil particle distribution is concentrated (non-uniform). Overall, the Δf values for soil particle distribution across the three soil layers from seven sampling events display a trend of decreasing

followed by an increase. This indicates that, over time, the concentration of soil particle distribution shifts from high before tillage to low after tillage, and then gradually returns to a state of high concentration with following irrigation and root growth. As the soil depth increases, this trend becomes less pronounced.

Based on the aforementioned analysis, it is evident that multifractal parameters such as D(1), ΔD, $\Delta\alpha$, and Δf can effectively characterize the distribution features of soil porosity at various levels, thus reflecting the uniformity of soil porosity distribution. To explore the relationships among these multifractal parameters, pairwise correlation analyses were conducted, and the results are presented in Table 1. The multifractal parameters exhibit substantial correlations, with correlation coefficients ($|r|$) ranging from 0.204 to 1.000. These parameters provide diverse perspectives on the heterogeneity of soil porosity distribution at different levels. In addition, $|r_{Layer1}| > |r_{Layer2}| > |r_{Layer3}|$, indicating that the multifractal parameters exhibit more pronounced patterns of variation concerning bulk density (γ).

Table 1. Pearson's correlation analysis between multifractal parameters and soil bulk density.

Layer		$D(1)$	ΔD	$\Delta\alpha$	$\Delta f(\alpha)$	γ
1	D(1)	1.000 **	−0.972 **	−0.972 **	−0.829 **	−0.748 **
	ΔD	−0.972 **	1.000 **	0.999 **	0.812 **	0.806 **
	$\Delta\alpha$	−0.972 **	0.999 **	1.000 **	0.830 **	0.809 **
	Δf(α)	−0.829 **	0.812 **	0.830 **	1.000 **	0.841 **
	γ	−0.748 **	0.806 **	0.809 **	0.841 **	1.000 **
2	D(1)	1.000 **	−0.966 **	−0.966 **	−0.810 **	−0.508 **
	ΔD	−0.966 **	1.000 **	0.999 **	0.843 **	0.539 **
	$\Delta\alpha$	−0.966 **	0.999 **	1.000 **	0.864 **	0.549 **
	Δf(α)	−0.810 **	0.843 **	0.864 **	1.000 **	0.651 **
	γ	−0.508 **	0.539 **	0.549 **	0.651 **	1.000 **
3	D(1)	1.000 **	−0.831 **	−0.825 **	−0.695 **	−0.204
	ΔD	−0.831 **	1.000 **	0.999 **	0.940 **	0.302 *
	$\Delta\alpha$	−0.825 **	0.999 **	1.000 **	0.950 **	0.346 *
	Δf(α)	−0.695 **	0.940 **	0.950 **	1.000 **	0.581 **
	γ	−0.204	0.302 *	0.346 *	0.581 **	1.000 **

Note: * indicates significance at the $p < 0.05$ level, and ** indicates significance at the $p < 0.01$ level.

4. Discussion

The soil particle-size distribution (Particle-SD) exhibits a spatial variability, with relatively insignificant temporal variations over a cropping season. In contrast, the distribution of soil pores demonstrates notable temporal fluctuations. Both the soil particle-size distribution (Particle-SD) and soil pore-size distribution (Pore-SD) adhere to a generalized power-law behavior, indicative of multifractal characteristics. The multifractal parameters of soil pore-size distribution are correlated with soil bulk density, and the order of correlation strength is $|r_{Layer1}| > |r_{Layer2}| > |r_{Layer3}|$.

In terms of spatial variation, our findings align with prior research: Both soil Particle-SD [28–30] and soil Pore-SD [11,19,31] exhibit spatial variability. However, with regard to temporal variation, the results of previous studies are divergent. Some researchers [2,12,32] posited that temporal variations exist in soil pore structure and soil moisture characteristic parameters. In particular, Bamberg [12] contended that soil properties are subject to variation, even over short time intervals, especially in managed soils. Nonetheless, Vogel [33] suggested that the pore structure is relatively static. It's important to note that Vogel's observations were primarily focused on soils with low organic matter content and low clay content, while the soils examined in this study were derived from the alluvial plains

of the Yellow River in the mid-lower reaches. Furthermore, Harold [34] proposed that soil structure changes periodically with field management. This study indicates that soil pore structure undergoes dynamic changes over a growing season. This prompts further speculation: could it be inferred that soil pores also exhibit variations during a single saturation–unsaturation process? If this hypothesis is substantiated, it suggests that the relationships within the soil water movement simulation, which employs the Richards equation, inherently encompass these changes via soil water retention curves. However, when employing a network model for soil water movement simulations, it is essential to note that soil pore networks are not static.

In the experiments, the particle size composition of the soil samples remained generally stable, with no significant temporal variability. However, changes in soil pore structure were observed, with a reduction in larger pores and a more pronounced decrease in smaller pores, indicating that the contraction of larger pores was less severe than that of smaller pores.

The experiment regarding the temporal variability of soil hydraulic parameters was conducted for a single growing season and was confined to a relatively limited spatial area of 200 m $\times$ 200 m. Both the temporal and spatial scopes were rather constrained. Subsequent investigations are planned to encompass a broader range of experiments focusing on the temporal variability of various soil parameters, accompanied by theoretical exploration.

In the context of simulating soil water movement during the crop season, it is proposed that introducing time-varying parameters for the soil water retention curve function $\Phi(\theta)$, particularly θs, α, and n, instead of the conventional fixed values, would provide a more accurate representation of real-world conditions, thus enhancing simulation precision. Furthermore, when employing data assimilation methods such as EnKF, incorporating time-varying parameters for $\Phi(\theta)$, including θs, α, and n, can accelerate model convergence and produce higher-precision assimilation results.

In this study, however, factors such as organic matter and mineral indicators were not considered in their impact on soil water movement parameters; the focus was solely on the physical parameters. Future research on the variability of soil water movement parameters should include considerations of organic matter, mineral indicators, and similar factors.

5. Conclusions

The soil particle-size distribution (Particle-SD) and soil pore-size distribution (Pore-SD) both adhere to a generalized power law, exhibiting multifractal characteristics. An analysis of soil pore distribution and the multifractal parameters of soil pore sizes indicates that soil pore distribution varies with factors such as tillage, irrigation, evaporation, and crop growth cycle. Additionally, multifractal parameters of soil pore-size distribution show correlations with soil bulk density, with the strength of these correlations ranked as |rLayer1| > |rLayer2| > |rLayer3|.

Based on the findings presented in this study, when conducting soil moisture transport simulations or data assimilation calculations under similar soil conditions in the region of the middle and lower reaches of the Yellow River, the utilization of time-varying soil moisture transport parameters can significantly enhance the precision of simulation outcomes.

Author Contributions: Conceptualization, Y.J. and X.S.; methodology, Y.J.; software, Y.F.; formal analysis, X.Z.; data curation, X.Z.; writing—original draft preparation, Y.J.; writing—review and editing, X.S.; visualization, Y.F.; project administration, X.S.; funding acquisition, X.S. All authors have read and agreed to the published version of the manuscript.

References

1. Du, T.; Li, D.; Guo, X.; Chen, S.; Sun, Q.; Yang, H.; Andales, A.A.; Wu, D. Linking Crop Water Productivity to Soil Physical, Chemical and Microbial Properties. *Front. Agric. Sci. Eng.* **2021**, *8*, 545–558. [CrossRef]

2. Roger-Estrade, J.; Richard, G.; Dexter, A.R.; Boizard, H.; Tourdonnet, S.; Bertrand, M.; Caneill, J. Integration of soil structure variations with time and space into models for crop management. A review. *Agron. Sustain. Dev.* **2009**, *29*, 135–142. [CrossRef]

3. Rabot, E.; Wiesmeier, M.; Schlüter, S.; Vogel, H.J. Soil structure as an indicator of soil functions: A review. *Geoderma* **2018**, *314*, 122–137. [CrossRef]

4. Yang, P.; Dong, W.; Heinen, M.; Qin, W.; Oenema, O. Soil Compaction Prevention, Amelioration and Alleviation Measures Are Effective in Mechanized and Smallholder Agriculture: A Meta-Analysis. *Land* **2022**, *11*, 645. [CrossRef]

5. Basset, C.; Abou Najm, M.; Ghezzehei, T.; Hao, X.; Daccache, A. How does soil structure affect water infiltration? A meta-data systematic review. *Soil Tillage Res.* **2023**, *226*, 105577. [CrossRef]

6. Ren, L.; Cornelis, W.M.; Ruysschaert, G.; De Pue, J.; Lootens, P.; D'Hose, T. Quantifying the impact of induced topsoil and historical subsoil compaction as well as the persistence of subsoiling. *Geoderma* **2022**, *424*, 116024. [CrossRef]

7. Yang, Y.; Wu, J.; Zhao, S.; Mao, Y.; Zhang, J.; Pan, X.; He, F.; Ploeg, M. Impact of long-term sub-soiling tillage on soil porosity and soil physical properties in the soil profile. *Land Degrad. Dev.* **2021**, *32*, 2892–2905. [CrossRef]

8. Liu, S.; Huang, Q.; Zhang, W.; Ren, D.; Xu, X.; Xiong, Y.; Huang, G. An improved estimation of soil water and salt dynamics by considering soil bulk density changes under freeze/thaw conditions in arid areas with shallow groundwater tables. *Sci. Total Environ.* **2023**, *859*, 160342. [CrossRef] [PubMed]

9. Dong, L.; Zhang, W.; Xiong, Y.; Zou, J.; Huang, Q.; Xu, X.; Ren, P.; Huang, G. Impact of short-term organic amendments incorporation on soil structure and hydrology in semiarid agricultural lands. *Int. Soil Water Conserv. Res.* **2022**, *10*, 457–469. [CrossRef]

10. Belik, A.A.; Kokoreva, A.A.; Bolotov, A.G.; Dembovetskii, A.V.; Kolupaeva, V.N.; Korost, D.V.; Khomyak, A.N. Characterizing macropore structure of agrosoddy-podzolic soil using computed tomography. *Open Agric.* **2020**, *5*, 888–897. [CrossRef]

11. Wang, Y.Q.; Shao, M.A. Spatial Variability of Soil Physical Properties in a Region of the Loess Plateau of Pr China Subject to Wind and Water Erosion. *Land Degrad. Dev.* **2011**, *24*, 296–304. [CrossRef]

12. Bamberg, A.L.; Cornelis, W.M.; Timm, L.C.; Gabriels, D.; Pauletto, E.A.; Pinto, L.F.S. Temporal changes of soil physical and hydraulic properties in strawberry fields. *Soil Use Manag.* **2011**, *27*, 385–394. [CrossRef]

13. Gerke, K.; Skvortsova, E.; Korost, D. Tomographic method ofstudying soil pore space: Current perspectives and results forsome Russian soils. *Eurasian Soil Sci.* **2012**, *45*, 781–791. [CrossRef]

14. Poppiel, R.R.; Paiva, A.F.d.S.; Demattê, J.A.M. Bridging the gap between soil spectroscopy and traditional laboratory: Insights for routine implementation. *Geoderma* **2022**, *425*, 116029. [CrossRef]

15. Wang, Q.; Horton, R.; Lee, J. A Simple Model Relating Soil Water Characteristic Curve and Soil Solute Breakthrough Curve. *Soil Sci.* **2002**, *167*, 436–443. [CrossRef]

16. Li, Q.; Zhang, J.; Zhou, F. Exact Solution for Capillary Bridges Properties by Shooting Method. *Z. Naturforsch.* **2017**, *72*, 315–320. [CrossRef]

17. Mandelbrot, B.B. *The Fractal Geometry of Nature*; W.H. Freeman: New York, NY, USA, 1982.

18. Mandelbrot, B.B. Intermittent turbulence in self-similar cascades: Divergence of high moments of the carrier. *J. Fluid Mech.* **1974**, *62*, 331–358. [CrossRef]

19. Burrough, P.A. Multiscale sources of spatial variation in soil. II. A non-Brownian fractal model and its application in soil survey. *J. Soil Sci.* **1983**, *34*, 599–620. [CrossRef]

20. Kravchenko, A.N.; Boast, C.W.; Bullock, D.G. Multifractal Analysis of Soil Spatial Variability. *Agron. J.* **1999**, *91*, 1033–1041. [CrossRef]

21. Mirás-Avalos, J.M.; Trigo-Córdoba, E.; da Silva-Dias, R.; Varela-Vila, I.; García-Tomillo, A. Multifractal behaviour of the soil water content of a vineyard in northwest Spain during two growing seasons. *Nonlinear Process. Geophys.* **2016**, *23*, 205–213. [CrossRef]

22. De, W.; Fu, B.; Zhao, W.; Hu, H.; Wang, Y. Multifractal characteristics of soil particle size distribution under different land-use types on the Loess Plateau, China. *Catena* **2008**, *72*, 29–36. [CrossRef]

23. Caniego, F.J.; Espejo, R.; Martín, M.A.; José, F.S. Multifractal scaling of soil spatial variability. *Ecol. Model.* **2005**, *182*, 291–303. [CrossRef]

24. Posadas, A.N.D.; Giménez, D.; Quiroz, R.; Protz, R. Multifractal Characterization of Soil Pore Systems. *Soil Sci. Soc. Am. J.* **2003**, *67*, 1361–1369. [CrossRef]

25. Fredlund, D.G.; Xing, A. Equations for the soil-water characteristic curve. *Can. Geotech. J.* **1994**, *31*, 521–532. [CrossRef]

26. Rényi, A. *Probability Theory*; North-Holland Publishing Company: Amsterdam, The Netherlands, 1970.

27. Everstz, C.J.G.; Mandelbrot, B.B. Multifractal measures. In *Chaos and Fractals*; Springer: Berlin/Heidelberg, Germany, 1992.

28. Wei, S.; Dai, Y.; Liu, B.; Ye, A.; Yuan, H. A soil particle-size distribution dataset for regional land and climate modelling in China. *Geoderma* **2012**, *171–172*, 85–91. [CrossRef]

29. Ghalib, A.M.; Hryciw, R.D. Soil Particle Size Distribution by Mosaic Imaging and Watershed Analysis. *J. Comput. Civ. Eng.* **1999**, *13*, 80–87. [CrossRef]

30. Zou, X.; Li, J.; Cheng, H.; Wang, J.; Zhang, C.; Kang, L.; Liu, W.; Zhang, F. Spatial variation of topsoil features in soil wind erosion areas of northern China. *Catena* **2018**, *167*, 429–439. [CrossRef]

31. Hendrayanto; Kosugi, K.i.; Uchida, T.; Matsuda, S.; Mizuyama, T. Spatial Variability of Soil Hydraulic Properties in a Forested Hillslope. *J. For. Res.* **1999**, *4*, 107–114. [CrossRef]

32. Huang, X.; Wang, H.; Zhang, M.; Horn, R.; Ren, T. Soil water retention dynamics in a Mollisol during a maize growing season under contrasting tillage systems. *Soil Tillage Res.* **2021**, *209*, 104953. [CrossRef]

33. Vogel, H.-J.; Roth, K. Quantitative morphology and network representation of soil pore structure. *Adv. Water Resour.* **2001**, *24*, 233–242. [CrossRef]

34. van Es, H.M. Evaluation of temporal, spatial, and tillage induced variability for parameterization of soil infiltration. *Geoderma* **1993**, *60*, 187–199. [CrossRef]